Laser Ablation Solid Sampling for Plasma Spectrochemistry

The Importance of Matching the Hardware to the Application

Lawrence Neufeld and John Roy

Careful consideration of the dynamics associated with laser ablation solid sampling systems ensures greater analytical precision and accuracy for ICP-MS/OES trace element analysis.

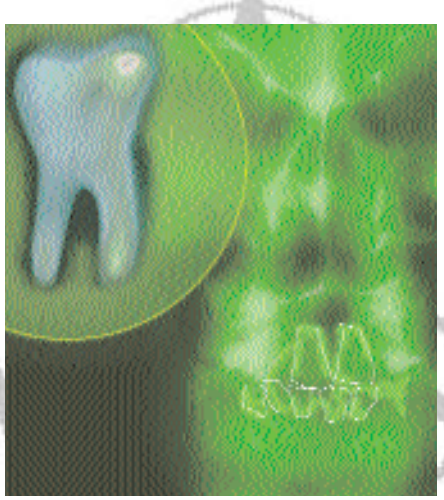

For many years, researchers have endeavored to determine the most effective method for collecting accurate in-situ data from solid sample matrices. Within the past 18 years, laser ablation (LA) solid sampling techniques have gained growing acceptance within the analytical community. Continued advances in hardware and analytical methodology bring us closer to our goal.

Some core issues need to be considered for LA. These parameters affect not only the dynamics of the ablation process itself, but also the transport and subsequent analysis of the sample aerosol by the analytical instrumentation. Currently three laser wavelengths are integrated into commercial systems designed as solid sample introduction devices. These three wavelengths are all in the short ultraviolet (UV) range of the spectrum: 266 nm, 213 nm, and 193 nm. The purpose of this article is to offer insight into the dynamics associated with a considered evaluation of this valuable technique.

In 1985 Gray (1) conducted experiments with a ruby laser at 694 nm. Arrowsmith (2) experimented with a 1064-nm laser, and Jenner and colleagues (3) incorporated a series of potassium di-deuterium phosphate crystals to generate 532-nm and 266-nm wavelengths. Geersten and colleagues (4) and Jefferies and colleagues (5) compared the fundamental Nd:YAG (neodymium:yttrium aluminum garnet) wavelength, 1064 nm, with its fourth harmonic at 266 nm. The shorter UV wavelengths displayed improved ablation characteristics and the general consensus today is that the UV wavelengths have many advantages over infrared and visible wavelengths for solid sampling applications across a wide range of materials. In 1997 Gunther and colleagues (6) published a paper based on work with an optically homogenized excimer laser, operating at 193 nm. They found that the benefits afforded by the short wavelength and even energy distribution of an optically homogenized beam were well suited to geochemical applications. These gas lasers, however, were larger, more expensive, and involved the frequent replacement of hazardous ArF gas. Jefferies and colleagues (7) compared the Nd:YAG fifth harmonic at 213 nm with

John Roy *
is vice president of New Wave Research, 47613 Warm Springs Blvd., Fremont, CA 94539. He can be reached via email at jroy@new-wave.com.

Lawrence Neufeld
is worldwide applications and marketing manager of laser ablation products at New Wave Research. He can be reached via email at lneufeld@new-wave.com.

*To whom all correspondence should be addressed.

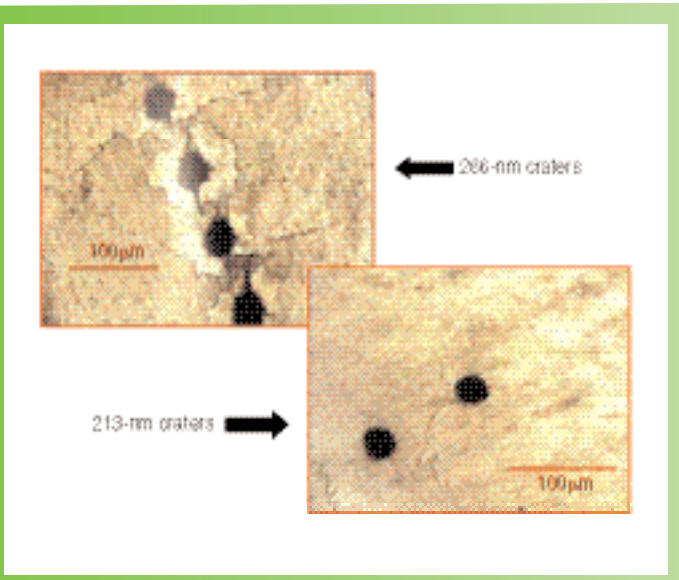

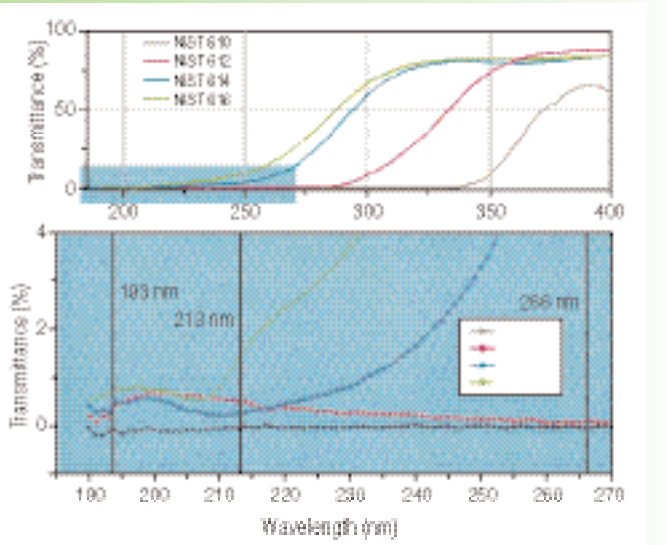

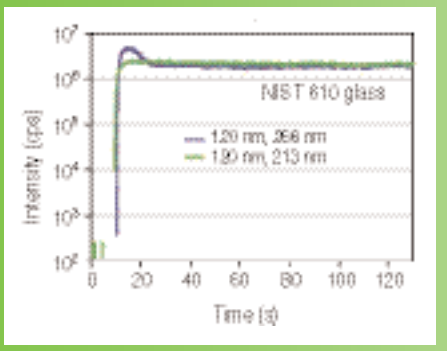

Figure 1 (upper left). Human teeth. Craters produced with the 213-nm laser system are relatively round and clean, whereas craters produced using the 266-nm wavelength are irregular and show excess ablated material around the sides of the craters.

Figure 2 (upper right). UV transmittance. Transmittance through all four NIST glasses by 193-nm, 213-nm, and 266-nm wavelengths. There is an apparent relationship between increasing transmittance of laser radiation through the sample matrix and larger aerosol particle size.

Figure 3(above). Single-spot ablation in NIST 610 glass. ^{232}Th plot of signal intensity, over time, showing a high-volume burst of material initially observed with the 266-nm laser system (green) which, when ablating glasses, subsequently falls to a plateau consistent with the 213-nm profile.

the Nd:YAG fourth harmonic at 266 nm and found a further benefit using the shorter 213-nm wavelength, especially when ablating traditionally difficult matrices. The analytical advantages of the 213-nm Nd:YAG appeared to be similar to those afforded by the excimer 193-nm laser, but in a simpler, more cost-effective design.

Today, LA as a sample introduction device for inductively coupled plasma–mass spectrometry (ICP-MS) has proved to be an invaluable tool for conducting trace element studies on a variety of solid materials (8–11). However, when visible lasers were first developed in the early 1980s as a sampling tool for atomic spectroscopy, it was clear that they had very limited capabilities compared with other techniques for analyzing solids (1). These limitations led researchers to investigate infrared (IR) lasers based on 1064-nm Nd:YAG technology (2). These systems initially showed a great deal of promise, but it soon became apparent that they did not meet the expectations of the trace element community, due to the inefficient absorption and unstable ablation of IR wavelengths in many solid matrices (1, 5, 12).

The basic limitations in IR laser technology led researchers to investigate the benefits of shorter, UV wavelengths. Systems were developed based on Nd:YAG technology, but using optical components to double (532 nm), quadruple (266 nm), and quintuple (213 nm) the frequency (3, 7). Innovations in lasing materials and electronic design together with better thermal characteristics produced higher energy with improved pulse-to-pulse stability. These new UV lasers showed significant improvements, particularly in the area of coupling efficiency, making them more suitable for a wider array of sample types — in particular, deep-UV wavelengths: 193-nm excimer lasers and 213-nm Nd:YAG lasers showed great promise as sampling devices for ICP-MS (6, 7).

The main advantage of short wavelength lasers is their better absorption capabilities in UV-transmissive materials like calcites, fluorites, and silicates, which make them ideally suited for geochemical studies. In addition they produce smaller particles and as a result generate an aerosol that is more effectively ionized when injected into an inductively coupled plasma (14, 15). There is also evidence to suggest that because the smaller particles are easier to volatize, they exhibit less elemental fractionation (time-dependent changes in elemental ratios) than longer UV, visible, and IR wavelengths.

The Evolution of Today's Laser Technology

The trace element community was looking for a routine technique that

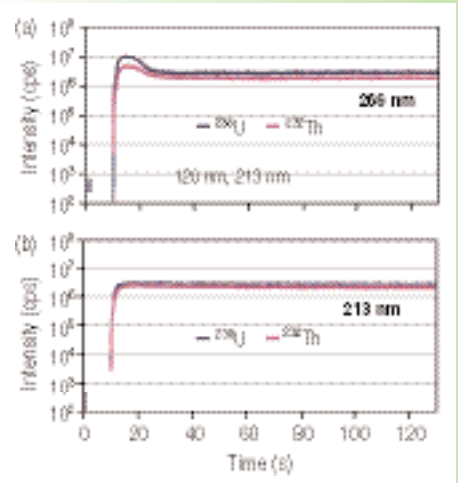

Figure 4 (right). Th/U fractionation in NIST 610 glass at (a) 266 nm and (b) 213 nm. The burst in signal correlates to the Th/U fractionation seen in the 266-nm chart and is due to the larger average particle size in the first 100 shots of 266 nm.

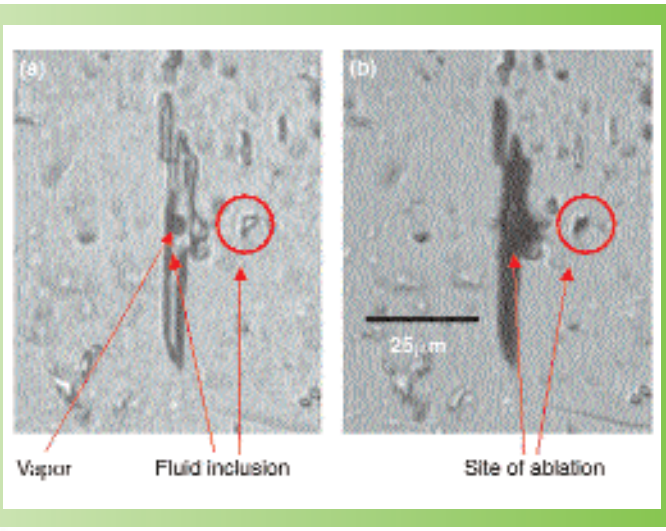

Figure 5 (upper right). Ablation of fluid inclusions. Visual magnification of two fluid inclusions, showing the inclusions (a) before and (b) after ablation using a 213-nm laser system. (Courtesy of Teresa Jeffries, National History Museum, London, United Kingdom.)

could replace some of the more traditional, solid sampling approaches, which were known to have limitations. It was another five years after the commercialization of the first Nd:YAG system that the next generation of LA systems was developed for use with ICP-MS. The new systems were based on Nd:YAG laser technology, but instead of using the fundamental 1064-nm wavelength, they used the fourth harmonic wavelength at 266 nm (3). These shorter-wavelength lasers proved to offer a significant improvement in performance over IR because they exhibited more controlled ablation characteristics than the fundamental wavelength (4, 18). This produced an aerosol of a more uniform particle size, which subsequently improved analytical precision. They also had much higher coupling efficiency, enabling controlled ablation of both transmissive and opaque materials such as glasses and other geological silicates. In addition, *internal homogenization* — a method to flatten the natural Gaussian nature of the Nd:YAG beam into a top-hat energy profile — led to an improvement in depth resolution and therefore better precision for small spot and depth profiling studies. This improvement in the laser energy profile, from Gaussian to flat, which was pioneered by Merchantek (acquired by New Wave Research [Fremont, CA] in 1999), also coincided with a new breed of ICP-MS instrumentation, which offered enhanced signal-to-noise ratios, improved tolerance to matrix components and better transient signal capability. The result was that LA-ICP-MS could now compete with other established techniques.

Benefits of Deep-UV Laser Technology

The commercial success of 266-nm lasers was primarily driven by geochemical applications. However, even though it was an excellent sampling tool for many diverse sample types, geochemists were the first group to realize its weaknesses. The inherent prob-

Figure 6 (below). Fish otolith – daily growth bands. With small, clean ablation lines (<10 μm width), it is possible to collect daily environmental data from the chemical composition of fish ear bones.

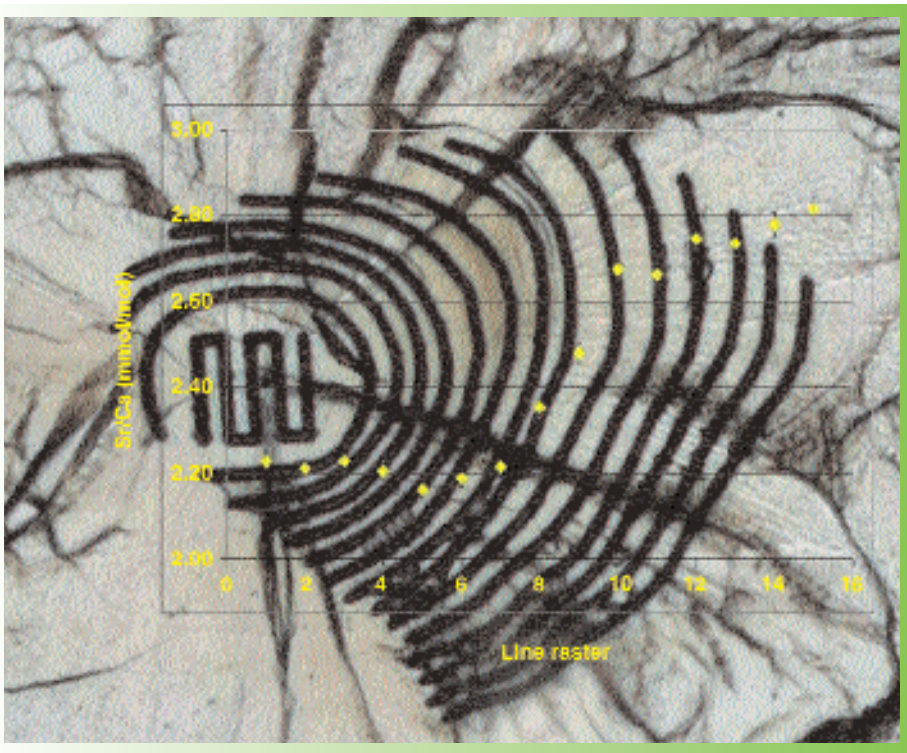

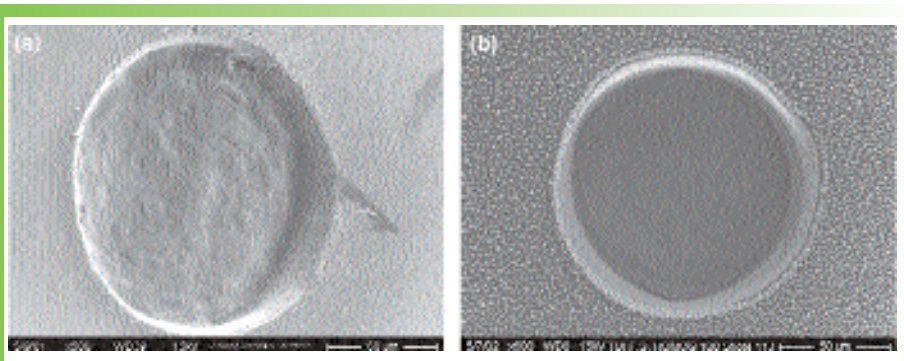

Figure 7 (left). Scanning electron microscope images of (a) a 213-nm Nd:YAG laser crater and (b) an optically homogenized flat-beam 193-nm ArF excimer laser crater.

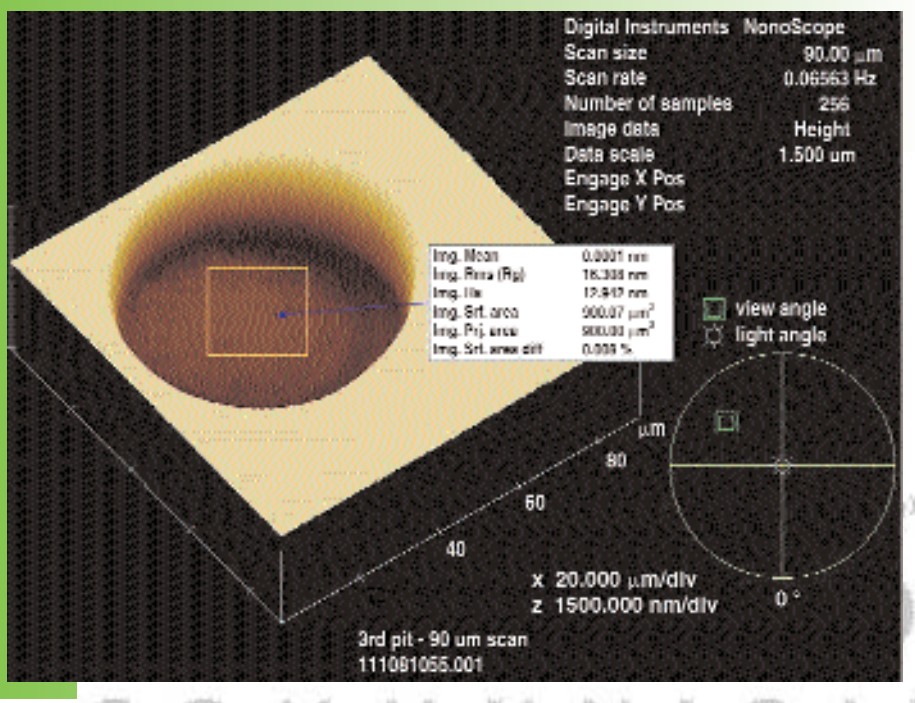

Figure 8. Atomic force microscopy image of a 193-nm crater in fused silica, produced by firing eight laser shots with an energy density of 30 J/cm^2 per shot.

lem lies in the fact that many geochemical studies involve the ablation of small spots and inclusions in UV-transmissive materials like silicates, calcite, and fluorite. Although 266-nm lasers can conduct in-situ analysis in many matrices well, the ablation process is not very controlled and precise when ablating materials with low UV absorbance. As a result, it is very difficult to ablate a minute area without removing some of the surrounding material (Figure 1). This inefficient coupling of the laser energy due to reduced absorbance initially generates larger particles (>1 µm size) and larger ablation volumes per shot, which are not efficiently ionized in the plasma and therefore contribute to poor precision (16, 19). In many materials, this effect diminishes with time as the laser "conditions" the matrix under the crater, decreasing the level of optical penetration (transparency) (13). This laser-induced opacity causes a longer wavelength, 266 nm, to behave like its shorter 213-nm cousin. These weaknesses in the 266-nm wavelength, most evident in geological applications, eventually led to the development of 213-nm lasers because of the recognized superiority of the shorter wavelengths to exhibit a higher degree of absorbance in UV transmissive matrices (7, 13, 20). It should be noted that for materials that are UV opaque (metal, plastic, biological, and so forth) the similarities between wavelengths are greater.

Laser Absorbance and Coupling Characteristics

Human teeth are composed primarily of an apatite matrix and grow approximately 30 µm per day. To acquire data with good temporal/spatial resolution in these samples, it is critical to produce small, clean ablation craters. It can be seen that the craters produced with the 213-nm wavelength have clean edges and are round and symmetrical, whereas the 266-nm craters are irregular and display fractures with ablated material splashed around the crater periphery (Figure 1). The temporal nature of the data becomes more ambiguous with increased fracturing and splattering of adjacent material on subsequent regions.

The more transmissive the sample matrix, the shorter the wavelength necessary for effective absorption of the laser energy (Figure 2). Figure 2 shows how the longer 266-nm wavelength is poorly absorbed in the low concentration standards NIST 614 and NIST 616, which are clear to the naked eye.

There is additional evidence that laser irradiance (fluence/pulse width), measured in GW/cm^2, may play a significant role in this process (21). This might explain why the 213-nm Nd:YAG laser operating at a maximum energy density of 25 J/cm^2 with a pulse width of 3 ns compares favorably with a 193-nm excimer laser operating at a maximum energy density of 45 J/cm^2 with a pulse width of 20 ns. The increased irradiance inherent in a short-pulse-width laser — 8.33 GW/cm^2 for the 213-nm wavelength versus 2.25 GW/cm^2 for the 193-nm wavelength — may play a role in improving the analytical capabilities of laser solid sampling (22).

The ablation characteristics responsible for the results displayed in Figure 1 are based on the relationship between laser wavelength, laser fluence (J/cm^2), laser pulse width, and laser transmittance through the sample matrix (23).

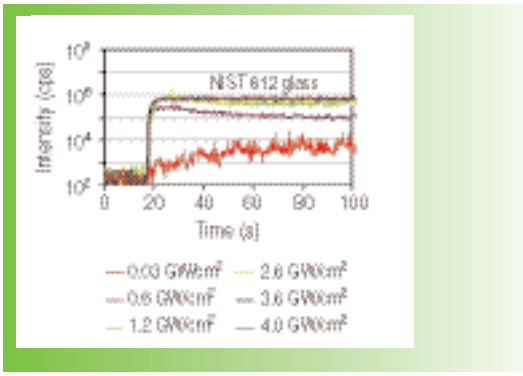

Figure 9. System flexibility and laser irradiance. As with any analytical tool, flexibility of design is critical for optimizing performance for a wide range of applications. With a large irradiance dynamic range (0.1 GW/cm^2 to $>$ 8.0 GW/cm^2) a stable aerosol can be obtained in virtually any matrix.

Besides a loss in spatial resolution, poor absorption of laser energy into certain sample matrices may be responsible for wide variations in ablation aerosol volume. The plot of a single-spot ablation in NIST 610 glass shown in Figure 3 displays the effect of increasing laser absorbance on ablated volume and has been seen by others (13, 16). Though the 213-nm spot rises rapidly to a stable plateau, the 266-nm wavelength spot presents a burst of particles to the ICP until sufficient damage is done to the matrix to make it more opaque to the 266-nm laser energy. This effect is directly related to laser energy absorbance and diminishes as the laser absorbance in the sample matrix increases.

In the great majority of LA applications, the dry aerosol removed from the sample is injected into an inductively coupled plasma. In ICP-MS the aerosol must be atomized and then ionized for it to pass through the mass spectrometer and be detected. If this process is incomplete, there will be poor correlation between atoms ablated and atoms detected, depending on the atomic or molecular volatility. If this inefficiency is consistent, it can be normalized over time with internal and external standards. However, if the relationship between atoms ablated and atoms detected changes with time (fractionation) as shown in Figure 4a, it is a more difficult problem.

As discussed earlier, the initial burst of ablated material with the 266-nm design generates a higher percentage of larger particles (>1 μm) (16). This relatively uncontrolled part of the ablation process displays a significant change in the volume and distribution of particles reaching the plasma. Due to the potential differences in volatilities of the elements and the inability of the plasma source to fully decompose large particles, particle-size–induced elemental fractionation effects are exaggerated at longer laser wavelengths.

This is demonstrated in Figure 4, which compares the ablation signals for ^{238}U with ^{232}Th in NIST 610 glass over the duration of 1200 laser shots (~2 min). The $^{238}U/^{232}Th$ ratio has been used by others because it is a good measure of particle-induced elemental fractionation (16). Uranium and thorium are approximately at equal concentration in NIST 610 glass and have similar ionization potentials. In Figure 4a the signal for the more volatile uranium is significantly higher than the signal for thorium in the first 200 shots of a 266-nm ablation. This effect can be directly correlated to the intensity burst displayed in Figure 3. In the 213-nm ablation profile (Figure 4b), the signals for both elements track each other for the entire 1200 laser shots.

It should be noted that other mechanisms can induce elemental fractionation (24–26). However, in this article we are only discussing particle-size–induced fractionation, which appears to be more sensitive to wavelength effects.

Because it is critical that these experiments are run under identical test conditions (other than wavelength), the data displayed in Figures 3 and 4 were acquired on the same LA system, incorporating the same optics and sample cell. Each experiment was run on the same day, analyzing NIST 610 glass by LA-ICP-MS within a few hours of each other. The only changes were to the harmonic crystals, converting from a 266-nm to a 213-nm configuration. Both laser power and spot sizes were measured at the sample to ensure experimental parity.

The continuous signals shown in Figures 3 and 4 were generated using 120-μm spot sizes, which is fairly common for bulk sampling. However, when micro inclusions or small spots are being studied, it is often necessary to sample areas that are well below 40 μm in diameter. These areas are so small that sometimes only a few laser pulses can be fired, each pulse having analytically useful information. A stable analyte signal throughout the entire ablation process is critical. For this type of work, short UV wavelengths (213 nm and 193 nm) offer clear advantages over the 266-nm design.

This is exemplified in Figure 5, which shows a screen shot of two fluid inclusions. Figure 5a is an image of the inclusions before ablation; Figure 5b shows the inclusions after ablation. The images and the ablation both came

from a Universal Platform 213-nm laser system, residing in Teresa Jefferies' lab at the Natural History Museum (London, United Kingdom). It is worth pointing out that the smaller inclusion (the one that's circled) is only 4 μm wide × 10 μm deep, and shows no sign of fracturing. Premature fracturing of the material surrounding an inclusion can cause a loss of critical analytical material, which is often under pressure. The uncontrolled ablation inherent in lasers having wavelengths poorly absorbed into surrounding matrix may cause such losses. In fact, this type of work would have been virtually impossible with older designs.

Fish otoliths (ear bones), similarly, require high spatial resolution. Daily growth bands are rarely wider than 20 μm and are typically between 4 μm–15 μm (9). For good temporal/spatial resolution, it is critical that small craters can be ablated in this delicate carbonate material (biogenic aragonite) (Figure 6).

Importance of Laser Beam Quality

The advantages of 213-nm laser technology strongly emphasize that matrix independence, high spatial resolution, and the ability to couple with UV transmissive materials without fracturing (particularly for small spots or depth analysis studies) were important for expanding the acceptance of LA solid sampling.

Excimer lasers (gas resonators) have been used by the semiconductor industry since the mid-1970s for etching silicone-based computer chips. As the density of these chips increased, so did the need to increase the spatial resolution of the laser lithography systems. By the 1990s, excimer lasers at 248 nm (KrF) and 193 nm (ArF) were being used for these applications. The matrix similarity between the silicon-based semiconductor applications and geological applications directed the analytical community toward excimer 193-nm laser systems to help overcome some of the problems associated with longer UV wavelengths (6, 29).

Besides the accepted superiority of the shorter 213-nm and 193-nm wavelengths to couple more efficiently to UV-transparent matrices, an added advantage of the 193-nm excimer design is that it uses the fundamental (unmodified) wavelength of an ArF gas laser and therefore achieves much higher energy transfer, compared with a Nd:YAG solid-state system that uses crystals to shorten the fundamental 1064-nm wavelength. Additionally, the less coherent nature of the excimer beam facilitates optical homogenization resulting in an extremely flat, even beam profile. The overall benefit is that cleaner, flatter craters are produced down to approximately 3–4 μm in diameter, at energy densities as great as 45 J/cm^2. This provides better control of the ablation process when depth profiling, or analyzing highly UV-transmissive materials. This is demonstrated in Figure 7, which shows scanning electron microscope images of a sample of glass ablated with a 213-nm Nd:YAG laser and

a crater ablated with a flat-beam 193-nm ArF excimer laser using an internally homogenized beam delivery system. The images show that the excimer laser produces a finer depth penetration profile than the Nd:YAG laser system.

In fact, an optically homogenized excimer laser beam is capable of producing single-shot crater profiles with <10 nm rms roughness, measured by an atomic force microscope. The image in Figure 8 is of a 193-nm crater in fused silica. The crater was produced by firing eight laser shots with an energy density of 30 J/cm^2 per shot using a UP193HE homogenized LA system (New Wave Research). The benefit of atomic force microscopy is that the topography of the crater can be accurately measured. The crater image shown in Figure 7 is 70 μm in diameter and 0.98 μm deep with a roughness at the bottom of only 16-nm rms.

New Opportunities for 266-nm Laser Technology

Even though the ablation characteristics of the 266-nm design are not as controlled as those of 213-nm and 193-nm technology, many applications do not require controlled ablation in UV-transmissive materials. Bulk analysis applications in opaque materials (plastic, metal, and biological) are benefiting from the improved design and analytical precision of specialized 266-nm LA systems. Applications for which bulk analysis or large-feature analysis (>50 μm) on the surface of solid samples is required are well suited to such systems. For these types of applications, a new breed of laser samplers are available, which are optimized for the ablation of larger volumes of material. Whether for use with an ICP-MS system to determine trace metals in high-purity alloys or to evaluate large surface features on a polymer using ICP–optical emission spectroscopy (OES), large–spot size 266-nm ablation has found its niche. Prospects for bulk laser sampling into an ICP-OES system are very promising because many alternative solid analysis techniques have limitations. For example, x-ray fluorescence (XRF) has detection capability limitations, arc/spark-

based instruments typically require an electrically conductive sample, and glow discharge techniques may produce very complex spectral information.

Importance of Selecting the Right Tool for the Job

A better understanding of the strengths and weaknesses of LA as a solid sampling tool has provided more clarity when choosing the best wavelength configuration for particular applications. Even though there might be some overlap, there is usually a clear choice based on the types of samples being analyzed, the trace element requirements and the data quality objectives.

Because there is a relationship between laser wavelength, laser irradiance, optical penetration depth, particle size, and analytical precision and accuracy, one must realize that many strategies are available to the laser chemist trying to acquire the best data with the hardware at hand. Many excellent papers have been written using all the wavelengths and system types described in this article. Creative, well thought out analytical methodology and system flexibility are what will enable analysts to reach their goals. Parameters such as laser irradiance (Figure 9) are important considerations whether operating at a 266-nm, 213-nm, or 193-nm wavelength. With flexible hardware design and an effective user interface, analysts should have the necessary tools.

The Final Analysis

There is no question that LA coupled to ICP-MS has proved itself to be an invaluable tool to carry out trace element studies directly on solid samples. It has the capability to analyze a diverse range of sample types, including the bulk analysis of plastics or compressed soils; the study of small spots or microinclusions on the surface of geological samples; thickness measurements of ceramic coatings; or even to be coupled to an ICP-OES instrument to analyze trace impurities in ceramics, and metallurgical samples. However, it is clear that not all laser systems offer the same ablation characteristics. Therefore, when evaluating the technique, careful consideration must be given to the elemental requirements, the type of samples being analyzed, and the data quality objectives of the analysis.

References

1. A.L. Gray, *Analyst* **110,** 551 (1985).
2. P. Arrowsmith, *Anal. Chem.* **59,** 1437 (1987).
3. G.A. Jenner, S.F. Foley, S.E. Jackson, T.H. Green, B.J. Fryer, and H.P. Longerich, *Cosmochim, Acta* **58,** 5099 (1994).
4. C. Geersten, A. Briand, F. Chartier, J.L. Lacour, P. Mauchien, S. Sjostrom, and J.M. Mermet, *J. Anal. Atom. Spectrometry* **9,** 17 (1994).
5. T.E. Jeffries, W.T. Perkins, and N.J.G. Pearce, *Analyst* **120,** 1365 (1995).
6. D. Gunther, R. Frischknecht, C.A. Heinrich, and H.J. Kahlert, *J. Anal. Atom. Spectrometry* **12,** 939 (1997).
7. T.E. Jeffries, S.E. Jackson, and H.P. Longerich, *J. Anal. Atom. Spectrometry* **13,** 935 (1998).
8. S.E. Jackson, H.P. Longerich, G.R. Dunning, and B.J. Fryer, *Canadian Mineralogist* **30,** 1049–1064 (1992).
9. S.R. Thorrold and S. Shuttleworth, *Can. J. Fish. Aquat. Sci.* **57,** 1232 (2000).
10. I. Horn, R.L. Rudnick, and W.F. McDonough, *Chemical Geology* **167,** 405 (2000).
11. G. Ghazi, S. Shuttleworth, R. Simmons, S.J. Paul, and D.H. Pashley, *J. Anal. Atom. Spectrometry* **17,** 1 (2002).
12. R.E. Wolf, C. Thomas, and A. Bohlke, *Appl. Surface Sci.* **127–129,** 299–303 (1998).
13. J. Gonzalez, X.L. Mao, J. Roy, S.S. Mao, and R.E. Russo, *J. Anal. Atom. Spectrometry* **17,** 1108 (2002).
14. S.H. Jeong, O.V. Borisov, J.H. Yoo, X.L. Mao, and R.E. Russo, *Anal. Chem.* **71,** 5123 (1999).
15. I. Horn and D. Gunther, *Appl. Surface Sci.* **9710,** 1 (2002).
16. M. Guillong and D. Gunther, *JAAS* **17,** 831 (2002).
17. E.R. Denoyer, K.J. Fredeen, and J.W. Hager, *Anal. Chem.* **63**(8), 445–457A (1991).
18. D. Figg and M.S. Kahr, *Appl. Spectrosc.* **51**(8), 1185, (1997).
19. D. Gunter and B. Hattendorf, *Mineralogical Association of Canada – Short Course Series* **29,** 83–91 (2001).
20. R.E. Russo, X.L. Mao, O.V. Borisov, and L. Haichen; *J. Anal. Atom. Spectrometry* **15,** 1115–1120 (2000).
21. H. Liu, O.V. Borisov, X. Mao, S. Shuttleworth, and R.E. Russo, *Appl. Spectrosc.* **54**(10), 1435 (2000).
22. R.E. Russo, X. Mao, and S.S. Mao, *Anal. Chem.* **74**(3), 70A (2002).
23. M. von Allman, *Laser-Beam Interactions with Materials – Physical Principles and Applications* (Springer Verlag, New York, 1987).
24. B.J. Fryer, S.E. Jackson, and H.P. Longerich, *Canadian Mineralogy* **33,** 303 (1995).
25. D.J. Figg, J.B. Cross, and C.H. Brink, *Appl. Surface Sci.* **127–129,** 287 (1998).
26. A.J.G. Mank and P.R.D. Mason, *J. Anal. Atom. Spectrometry* **14,** 1143 (1999).
27. S.J. Holmes, P.H. Mitchell, H.C. Hakey, *Optical Lithography* **41**(1/2), 49 (1997).
28. M. Rothschild, A.R. Forte, R.R. Kunz, S.C. Palmateer, and J.H.C. Sedlacek, *Optical Lithography* **41**(1/2), 49 (1997).
29. S.M. Eggins, L.P.J. Kinsley, and J.M.G. Shelley, *Appl. Surface Sci.* **127–129,** 278 (1998).
30. S.F. Durrant, *J. Anal. Atom. Spectrometry* **14,** 1385 (1999). ■